IR and Raman spectra of nitroanthracene isomers: Substitional effects based on density functional theory study

ARTICLE *in* SPECTROCHIMICA ACTA PART A MOLECULAR AND BIOMOLECULAR SPECTROSCOPY · APRIL 2012

Impact Factor: 2.35 · DOI: 10.1016/j.saa.2011.12.052 · Source: PubMed

2 AUTHORS:

Andrea Alparone
University of Catania
67 PUBLICATIONS **791** CITATIONS
SEE PROFILE

Vito Librando
University of Catania
144 PUBLICATIONS **1,261** CITATIONS
SEE PROFILE

Spectrochimica Acta Part A 89 (2012) 129–136

Contents lists available at SciVerse ScienceDirect

Spectrochimica Acta Part A: Molecular and Biomolecular Spectroscopy

journal homepage: www.elsevier.com/locate/saa

IR and Raman spectra of nitroanthracene isomers: Substitional effects based on density functional theory study

Andrea Alparone [a], Vito Librando [a,b,*]

[a] Research Centre for Analysis, Monitoring and Minimization Methods of Environmental Risk, viale A. Doria 6, Catania 95125, Italy
[b] Department of Chemistry, University of Catania, viale A. Doria 6, Catania 95125, Italy

ARTICLE INFO

Article history:
Received 21 September 2011
Received in revised form
27 November 2011
Accepted 21 December 2011

Keywords:
Nitroanthracenes
IR and Raman spectra
Density functional theory
Environmental pollutants
Mutagenic activity

ABSTRACT

Structure, IR and Raman spectra of 1-, 2- and 9-nitroanthracene isomers (**1-NA**, **2-NA** and **9-NA**) were calculated and analyzed through density functional theory computations using the B3LYP functional with the 6-311 + G** basis set. Steric and π-conjugative effects determine the characteristic O—N—C—C dihedral angles, which vary from 0° (**2-NA**) to 28-29° (**1-NA**) and 59° (**9-NA**), influencing the relative order of stability along the series **9-NA** < **1-NA** < **2-NA**. The spectral regions at wavenumber values >3000 cm^{-1} and <1000 cm^{-1} little depend on the substituent position. The Raman and IR intensity values of the characteristic symmetric nitro group stretching transition, appearing between 1310 and 1345 cm^{-1}, are rather sensitive to the position of the substituent, decreasing regularly on passing from the planar to the NO_2-rotated isomers (**9-NA** < **1-NA** < **2-NA**). In the medium-energy spectral region (1000–1700 cm^{-1}), the number and the relative position of the strongest Raman bands are of potential utility to discriminate the **NA** isomers. Structural and spectroscopic results suggest that the unknown mutagenic activity of **1-NA** is expected to be between that of **9-NA** and **2-NA**.

1. Introduction

Nitroanthracenes (**NA**s) belong to a class of widely distributed environmental contaminants known as nitrated polycyclic aromatic hydrocarbons (NPAHs) [1–5]. NPAHs are usually released in the environment during incomplete combustion processes or by reaction between polycyclic aromatic hydrocarbons (PAHs) and nitrogen oxides present in the atmosphere [5–8]. Many NPAHs exhibit extremely high mutagenic and carcinogenic potencies, often greater than those of their parents PAHs [2–4]. It is well recognized that mutagenic and carcinogenic activities of NPAHs are dramatically affected by the structure. Planar NPAHs exhibit higher mutagenic potencies than the corresponding isomers with the nitro group oriented perpendicularly to the aromatic moiety [2–4].

Nitroanthracenes exist as three isomers (Fig. 1): **1-NA** and **9-NA** are predicted to be non planar, while **2-NA** exhibits a planar arrangement. Experimental structures of **NA**s are not available in the literature, except for the geometry of **9-NA** in the solid [9]. This isomer characterized by the NO_2 group arranged perpendicularly to the aromatic plane, is a prototypical molecule for the study of photochemical degradation reactions [10–13]. Photodegradation mechanisms are by far the most important natural phenomena of removal of NPAH pollutants in the environment [4]. On the theoretical side, semiempirical PM3 [14] and density functional theory (DFT) structures of **NA**s [15] were previously reported, while Lee et al. [16] computed the electronic second-order hyperpolarizability by using a finite-field procedure. The different retention times for **2-NA** and **9-NA** as determined by HPLC analyses are consistent with their distinct structure and dipolar character [17].

The mutagenic activities of the **NA** isomers are somewhat different to each other. On the basis of the Ames test, which commonly uses the *Salmonella typhimurium* strains TA98 and TA100, **2-NA** is estimated to be three order of magnitudes more mutagenic than **9-NA** [18–22]. The mutagenic potency for **1-NA** is unknown so far. Therefore it is of great importance to identify analytic methodologies suitable to discriminate structurally different isomers. To this purpose, IR and Raman spectroscopies can be very helpful. Vibrational spectra can be accurately simulated through high-level quantum mechanical calculations [23,24].

In the present work, we determined and analyzed the vibrational spectra for the series of the **NA** isomers by using DFT computations. The spectroscopic properties and complete normal mode assignments are reported here for the first time. To our knowledge, some experimental wavenumber values are available only for **2-NA** [25] and **9-NA** [26]. The main goal of this work is to explore the effects of the position of the substituent on the IR and

* Corresponding author at: Research Centre for Analysis, Monitoring and Minimization Methods of Environmental Risk, viale A. Doria 6, Catania 95125, Italy. Tel.: +39 95 7385201; fax: +39 95 580138.
E-mail address: vlibrando@unict.it (V. Librando).

1386-1425/$ – see front matter © 2011 Elsevier B.V. All rights reserved.
doi:10.1016/j.saa.2011.12.052

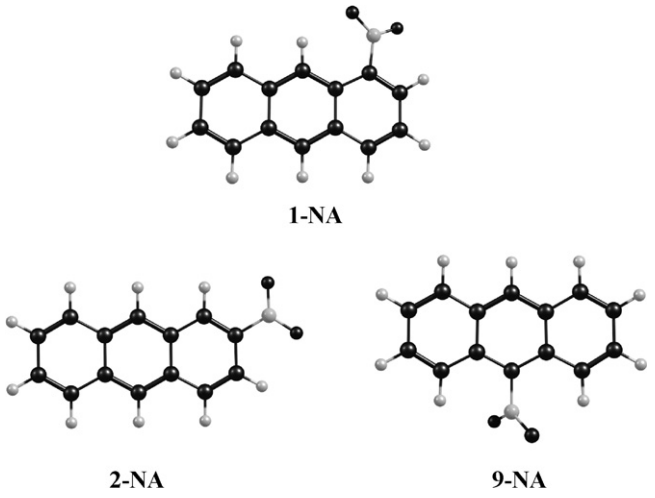

Fig. 1. Structure of nitroanthracene isomers.

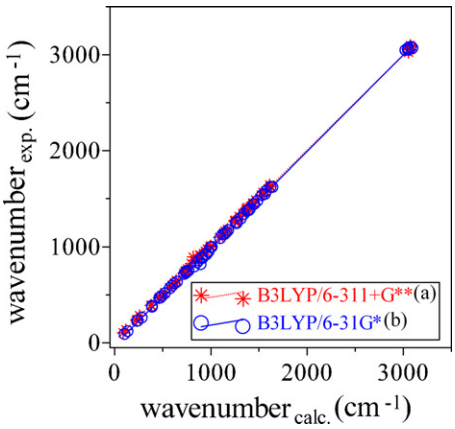

Fig. 2. Experimental [47] *vs.* calculated wavenumbers relationships for anthracene. (a) $\text{wavenumber}_{exp.} = 21.51 + 0.99 \times \text{wavenumber}_{calc.}$, $r^2 = 1.00$; (b) $\text{wavenumber}_{exp.} = -21.89 + 1.01 \times \text{wavenumber}_{calc.}$, $r^2 = 1.00$.

Raman spectra, in order to identify vibrational markers potentially useful to distinguish the **NA** isomers.

2. Computational details

All computations were performed with the Gaussian 03 program [27]. The ground-state geometries of the **NA** isomers were optimized by using the DFT-B3LYP functional [28,29] with the 6-31G* and 6-311 + G** basis sets. IR and Raman spectra were calculated under the harmonic approximation at the B3LYP/6-31G* and B3LYP/6-311 + G** levels using the geometries computed at the same levels. The absence of imaginary wavenumber values confirms that all the structures correspond to equilibrium minima on the potential energy surfaces. In general DFT harmonic treatments overestimate observed vibrational wavenumbers owing to neglecting of anharmonic corrections, incompleteness of basis set and electron correlation contributions. These discrepancies are commonly corrected either by computing explicitly anharmonic terms [30,31] or by performing scaled quantum mechanical force field procedures [32], or directly by scaling the calculated wavenumbers with a given factor [33]. For this series of compounds anharmonic treatments are computationally impracticable and therefore we adopted the scaling approach employing a single factor of 0.9594 and 0.9679, specifically determined for the B3LYP/6-31G* [33] and the B3LYP/6-311 + G** [34] levels of calculation, respectively. This approach was proven to give good results for the vibrational spectra of substituted PAHs [35–42]. Complete vibrational assignments were carried out on the basis of normal modes, as displacements in redundant internal coordinates (in Gaussian 03, option Freq = IntModes) and also by means of the visualization software Chemcraft [43].

3. Results and discussion

The experimental geometry is available only for **9-NA** from X-ray measurements [9]. As can be seen from the data reported in Table 1, the B3LYP/6-311 + G** level furnishes the best results, in agreement with the comparison between the observed [44] and calculated data of nitrobenzene (**NB**). For **9-NA** the B3LYP/6-31G* and B3LYP/6-311 + G** computations, respectively, underestimate the experimental C—N bond length by 0.010 and 0.003 Å, the O—N—C—C dihedral angles by 34° and 26°, while overestimate the O—N bond length by 0.016 and 0.009 Å. These differences can be principally attributed to crystal packing effects. In fact, in carbon tetrachloride solution the O—N—C—C dihedral angle for the most stable configuration of **9-NA** was estimated to be 64° [26], somewhat close to the gas phase B3LYP/6-311 + G** datum. At the B3LYP/6-311 + G** level on passing from **2-NA** to **1-NA** and **9-NA** the C—N bond length increases by 0.003 and 0.005 Å, respectively. In addition, the O—N—C—C dihedral angles, which crucially characterize the structure of NPAHs, are calculated to be 28° and 29°, 0° and 0°, 59° and 59° for **1-NA**, **2-NA, 9-NA**, respectively. The relative stability for the **NA** isomers computed at the B3LYP/6-311 + G** level decreases in the order (in parentheses is reported the relative energy corrected for the zero-point vibrational contribution expressed in kJ/mol):

$$\mathbf{2\text{-}NA}(0.0) > \mathbf{1\text{-}NA}(18.5) > \mathbf{9\text{-}NA}(30.9)$$

The corresponding values computed at the B3LYP/6-31G* level are rather similar, being 0.0, 17.9 and 32.9 kJ/mol, respectively. This trend is consistent with the structural data and is consequence of the steric repulsions between the hydrogen atoms and the closest oxygen atoms for the NO_2-rotated structures, which decrease the π-conjugative interaction between the nitro group and the aromatic moiety.

To the best of our knowledge experimental and theoretical vibrational studies of **NA**s are not available, except for a SERS study of **9-NA** [45], FT-IR and FT-Raman spectra of **2-NA** [25] and the vibrational wavenumber values for the NO_2 symmetric stretching vibration of **9-NA** in carbon tetrachloride solution and solid phases [26]. However, complete normal mode assignments are lacking so far. On the other hand, several experimental and theoretical vibrational spectra of the parent compounds anthracene (**A**) [46–48] and **NB** [49] are known and were here employed to validate the theoretical approach. Present simulated spectra were obtained by convoluting the computed wavenumber values using pure Lorentzian band shapes with a full width at half maximum of 10 cm^{-1}, as commonly adopted in the literature [50–55].

3.1. IR and Raman spectra of anthracene and nitrobenzene

The B3LYP/6-311 + G** wavenumber, IR intensity (I_{IR}) and Raman activity (A_{Raman}) values for **A** and **NB** are listed in Tables 2 and 3, respectively, together with the available experimental data reported in Refs. [47] and [49]. Present corrected wavenumber values are in reasonable agreement with both experimental and previous DFT data [46–49] (Figs. 2 and 3). In comparison to the observed wavenumber values, a root-mean-square deviation of 19 cm^{-1} is found for both **A** and **NB** (20 cm^{-1} using the less expensive B3LYP/6-31G* level), which raises to 45 and 49 cm^{-1} in the case of the uncorrected data, respectively.

Table 1
Selected geometrical parameters for nitrobenzene (**NB**) and 9-nitroanthracene (**9-NA**).

	C—N (Å)	O—N (Å)	O—N—O (°)	O—N—C—C (°)
NB				
B3LYP/6-31G*	1.473	1.231	125	
B3LYP/6-311 + G**	1.480	1.225	125	
Exp. [a]	1.486	1.223	125	
9-NA				
B3LYP/6-31G*	1.472	1.232	124	51
B3LYP/6-311 + G**	1.479	1.225	125	59
Exp. [b]	1.482	1.216	124	85

[a] Electron diffraction values from [44].
[b] X-ray diffraction values from [9].

The B3LYP/6-311 + G** IR and Raman spectra of **A** in the 600–1700 cm^{-1} wavenumber range are displayed in Fig. 4. In line with the experimental IR spectrum [47], the low-energy spectral region is characterized by two intense absorptions here placed at 870 cm^{-1} (mode no. 42, I_{IR} = 62.2 km/mol) and 716 cm^{-1} (mode no. 50, I_{IR} = 91 km/mol). Both these vibrations are attributed to out-of-plane bending deformations (γC—Hs, Fig. 5). The corresponding observed figures are 876 and 725 cm^{-1}, respectively, the calculated wavenumber values being in error by 0.7 and 1.2%, respectively. The simulated Raman spectrum shows an isolated strong peak at 1381 cm^{-1} (A_{Raman} = 936 $Å^4$/amu), to be compared with the experimental wavenumber value of 1408 cm^{-1}. This transition is assigned to a symmetrical ring stretching vibration (νring, mode no. 19, Fig. 5c) and is not visible in the IR spectrum.

The simulated vibrational spectra of **NB** between 600 and 1700 cm^{-1} are displayed in Fig. 6. The IR spectrum is characterized by two almost equally intense absorptions here placed at 1532 cm^{-1} (mode no. 8, I_{IR} = 255 km/mol) and 1327 cm^{-1} (mode no. 11, I_{IR} = 295 km/mol). These transitions are ascribed to the asymmetric ($\nu_a NO_2$) and symmetric ($\nu_s NO_2$) N—O bonds stretching vibrations, respectively, the former showing also a non-negligible contribution from a νring motion. Note that the corresponding observed figures are placed at 1523 and 1347 cm^{-1} [49], the B3LYP/6-311 + G** data being in error by 0.6 and 1.5%, respectively. As can been from Fig. 6 the calculated Raman spectrum is dominated by the $\nu_s NO_2$ transition (1327 cm^{-1}).

The above results suggest that, in line with usual literature data, the employed B3LYP/6-311 + G** theoretical treatment is expected to work suitably also for the vibrational properties of **NA**s.

Table 2
Calculated vibrational wavenumbers (cm^{-1}), IR intensities, I_{IR} (km/mol) and Raman activities, A_{Raman} ($Å^4$/amu) of anthracene. B3LYP/6-311 + G** results.

No.	Symm.	Calc.				Exp.[a]	No.	Symm.	Calc.				Exp.[a]
		Wav.[b]	I_{IR}	A_{Raman}	Descr.[c]	ν			Wav.[b]	I_{IR}	A_{Raman}	Descr.[c]	Wav.
1	A_g	3085.3	0.0	791.4	νC—H		34	B_{2u}	992.5	8.6	0.0	δC—H	1000
2	B_{2u}	3085.0	51.8	0.0	νC—H	3081	35	B_{2g}	964.6	0.0	1.1	γC—H	975
3	B_{1u}	3073.6	59.4	0.0	νC—H	3098	36	A_u	964.0	0.0	0.0	γC—H	979
4	B_{3g}	3073.4	0.0	236.3	νC—H	3054	37	B_{3u}	946.7	5.8	0.0	γC—H	953
5	A_g	3061.9	0.0	345.6	νC—H	3056	38	B_{1g}	941.8	0.0	5.0	γC—H	956
6	B_{2u}	3060.5	0.0	0.0	νC—H	3050	39	B_{3g}	899.0	0.0	0.1	δring	912
7	B_{1u}	3057.0	13.0	0.0	νC—H	3057	40	B_{1u}	888.8	1.9	0.0	δring	907
8	B_{3g}	3056.1	0.0	15.2	νC—H		41	B_{2g}	881.6	0.0	0.4	γC—H	916
9	A_g	3054.4	0.0	49.1	νC—H	3027	42	B_{3u}	869.6	62.2	0.0	γC—H	876
10	B_{1u}	3052.5	7.7	0.0	νC—H	3025	43	A_u	836.7	0.0	0.0	γC—H	860
11	B_{1u}	1612.9	4.3	0.0	νring	1624	44	B_{2g}	815.2	0.0	0.1	γC—H	896
12	B_{3g}	1611.4	0.0	0.6	νring	1643	45	B_{2u}	793.9	0.1	0.0	δring	828
13	B_{3g}	1568.5	0.0	9.7	νring	1576	46	B_{2g}	756.1	0.0	0.8	γC—H	771
14	A_g	1540.6	0.0	95.1	νring	1566	47	B_{1g}	744.6	0.0	1.1	γC—H	747
15	B_{2u}	1526.1	6.8	0.0	νring	1536	48	A_g	738.3	0.0	75.0	δring	753
16	A_g	1466.2	0.0	132.0	δC—H	1486	49	A_u	731.0	0.0	0.0	γC—H	744
17	B_{1u}	1436.8	1.4	0.0	δC—H	1454	50	B_{3u}	716.0	91.2	0.0	γC—H	725
18	B_{2u}	1432.7	1.2	0.0	δC—H	1447	51	B_{1u}	639.6	0.6	0.0	δring	651
19	A_g	1380.6	0.0	935.7	νring	1408	52	A_g	620.9	0.0	1.5	δring	624
20	B_{2u}	1369.0	1.6	0.0	δC—H	1398	53	B_{2u}	597.0	8.4	0.0	δring	601
21	B_{3g}	1367.9	0.0	3.0	δC—H	1382	54	B_{2g}	570.7	0.0	0.0	τring	577
22	B_{2u}	1331.0	4.1	0.0	δC—H	1346	55	B_{3g}	517.9	0.0	12.0	δring	524
23	B_{1u}	1294.2	4.8	0.0	δC—H	1315	56	A_u	490.2	0.0	0.0	τring	493
24	B_{3g}	1253.1	0.0	0.0	δC—H	1274	57	B_{1g}	469.5	0.0	2.0	τring	477
25	B_{1u}	1248.7	5.5	0.0	δC—H	1271	58	B_{3u}	461.4	26.6	0.0	τring	468
26	A_g	1246.7	0.0	72.0	δC—H	1263	59	A_g	384.7	0.0	27.9	δring	390
27	B_{3g}	1171.4	0.0	29.9	δC—H	1183	60	B_{3g}	382.9	0.0	4.8	δring	391
28	A_g	1151.5	0.0	6.8	δC—H	1165	61	B_{3u}	375.0	0.0	0.0	τring	391
29	B_{2u}	1150.2	1.6	0.0	δC—H	1165	62	B_{2g}	257.7	0.0	0.0	τring	284
30	B_{1u}	1134.8	7.9	0.0	δC—H	1148	63	B_{1g}	228.0	0.0	1.7	τring	242
31	B_{2u}	1121.5	1.8	0.0	δC—H	1124	64	B_{1u}	227.9	1.5	0.0	δring	235
32	B_{3g}	1089.3	0.0	0.1	δC—H	1100	65	A_u	115.6	0.0	0.0	τring	137
33	A_g	996.8	0.0	81.1	δC—H	1012	66	B_{3u}	87.3	1.4	0.0	τring	105

[a] Experimental data taken from Ref. [47].
[b] Harmonic values corrected by a scaling factor of 0.9679 taken from Ref. [34].
[c] ν = stretching, δ = in-plane bending, γ = out-of-plane bending, τ = torsion. The relative weights of the geometrical parameters for each normal vibrational mode are given in Table S1of the Supplementary data.

Table 3
Calculated vibrational wavenumbers (cm^{-1}), IR intensities, I_{IR} (km/mol) and Raman activities, A_{Raman} ($Å^4$/amu) of nitrobenzene. B3LYP/6-311 + G** results.

No.	Symm.	Calc.				Exp.[a]
		Wav.[b]	I_{IR}	A_{Raman}	Descr.[c]	Wav.
1	A_1	3119.5	5.0	152.5	νC—H	3107
2	B_2	3119.2	0.7	9.6	νC—H	3107
3	A_1	3093.2	8.0	179.7	νC—H	3076
4	B_2	3084.8	9.2	89.4	νC—H	3076
5	A_1	3072.4	0.7	57.3	νC—H	3049
6	B_2	1598.7	33.4	0.0	νring + $\nu_a NO_2$	1620
7	A_1	1575.6	3.5	69.8	νring	1588
8	B_2	1532.0	255.2	19.4	$\nu_a NO_2$ + νring	1523
9	A_1	1460.0	9.4	0.7	δC—H	1479
10	B_2	1438.6	0.1	0.0	δC—H	1455
11	A_1	1327.0	294.8	168.2	$\nu_s NO_2$	1347
12	B_2	1309.8	14.3	1.1	νring	1316
13	B_2	1293.9	0.2	0.1	δC—H	1308
14	A_1	1157.2	2.8	3.5	δC—H	1174
15	B_2	1146.7	0.7	5.3	δC—H	1162
16	A_1	1079.4	37.3	41.9	δring + νCN	1108
17	B_2	1064.1	9.3	0.0	δC—H	1070
18	A_1	1008.3	6.5	14.7	δC—H	
19	A_1	985.7	0.3	34.3	δring	1004
20	B_1	984.8	0.1	0.1	γC—H	1021
21	A_2	969.2	0.0	0.0	γC—H	990
22	B_1	927.9	4.0	0.0	γC—H	975
23	A_1	840.6	34.2	12.8	σNO_2	852
24	A_2	829.1	0.0	0.2	γC—H	840
25	B_1	761.4	32.3	1.2	γC—H	793
26	B_1	683.2	59.3	0.2	γC—H	702
27	A_1	673.8	8.2	1.9	δring	681
28	B_1	655.0	13.5	0.0	γC—H	676
29	B_2	606.4	0.0	6.0	δring	611
30	B_2	509.5	1.2	2.7	δring	532
31	B_1	424.9	1.1	0.0	τring	436
32	A_2	402.7	0.0	0.0	τring	417
33	A_1	382.2	0.9	2.7	δring	392
34	B_2	247.8	1.0	0.5	δring	255
35	B_1	163.0	0.9	1.7	τring	182
36	A_2	47.5	0.0	0.0	τNO_2	51

[a] Experimental data taken from [49].
[b] Harmonic values corrected by a scaling factor of 0.9679 taken from Ref. [34].
[c] ν = stretching, δ = in-plane bending, γ = out-of-plane bending, σ = scissoring, τ = torsion, a = antisymmetric, s = symmetric. The relative weights of the geometrical parameters for each normal vibrational mode are given in Table S2 of the Supplementary data.

3.2. IR spectra of nitroanthracenes

The B3LYP/6-311 + G** wavenumber and I_{IR} values for **NA**s are reported in Tables 4–6, together with an approximate description of the normal modes. For every **NA** isomer in total there are 72 vibrations in the wavenumber range from 3127 to 41 cm^{-1}. In the highest-wavenumber spectral region (wavenumbers > 3000 cm^{-1}), the C—H stretching transitions are located in the 3127–3059 cm^{-1} wavenumber range. However, these absorption bands are not appreciably affected by the position of the substituent, being of little utility to discriminate the investigated isomers. For all the **NA**s a very intense IR absorption is located in the medium-energy

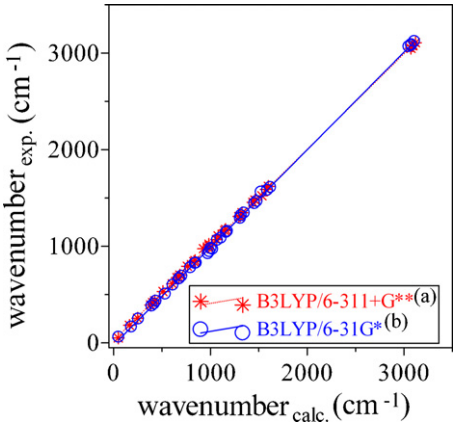

Fig. 3. Experimental [49] *vs.* calculated wavenumbers relationships for nitrobenzene. (a) $wavenumber_{exp.} = 24.78 + 0.99 \times wavenumber_{calc.}$, $r^2 = 1.00$; (b): $wavenumber_{exp.} = -22.09 + 1.01 \times wavenumber_{calc.}$, $r^2 = 1.00$.

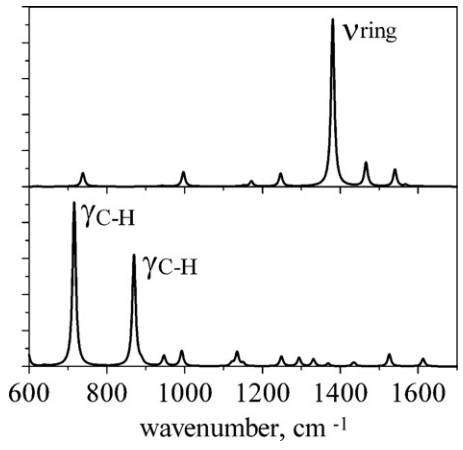

Fig. 4. Calculated B3LYP/6-311 + G** IR (bottom) and Raman (top) spectra of anthracene.

Table 4
Calculated vibrational wavenumbers (cm^{-1}), IR intensities, I_{IR} (km/mol) and Raman activities, A_{Raman} ($Å^4$/amu) of 1-nitroanthracene. B3LYP/6-311 + G** results.

No.	Wav.[a]	I_{IR}	A_{Raman}	Descr.[b]	No.	Wav.[a]	I_{IR}	A_{Raman}	Descr.[b]
1	3127.1	2.1	54.6	νC—H	37	957.1	27.3	11.8	νC—N
2	3114.7	1.7	150.6	νC—H	38	950.3	2.8	2.3	γC—H
3	3090.8	11.9	230.6	νC—H	39	920.4	2.1	1.2	γC—H
4	3088.2	21.9	370.2	νC—H	40	898.2	1.8	0.2	δring
5	3077.7	21.2	116.6	νC—H	41	888.3	19.7	3.8	γC—H
6	3068.6	5.2	127.4	νC—H	42	871.2	34.7	0.4	γC—H
7	3066.6	0.4	81.4	νC—H	43	852.0	8.6	0.7	δring
8	3061.2	3.4	38.7	νC—H	44	831.1	1.9	0.8	γC—H
9	3059.0	1.5	14.0	νC—H	45	801.6	11.9	3.9	σNO_2
10	1614.0	4.9	2.1	νring	46	789.4	6.3	1.2	γC—H
11	1608.7	23.7	65.3	νring	47	758.5	5.8	80.9	δring
12	1569.0	6.4	11.5	νring	48	743.2	0.4	1.5	γC—H
13	1538.5	14.5	182.2	νring	49	739.8	9.3	6.1	γC—H
14	1528.3	63.9	27.8	νring	50	720.8	55.6	5.4	γC—H
15	1514.8	193.1	68.2	$\nu_a NO_2$	51	710.5	13.6	0.4	γC—H
16	1461.8	6.5	98.8	δC—H	52	661.4	7.4	5.7	δring
17	1436.3	1.7	2.2	δC—H	53	642.8	0.7	1.1	δring
18	1417.1	5.2	1.0	δC—H	54	610.6	4.6	1.7	δring
19	1383.9	11.9	856.9	νring	55	576.8	1.0	1.8	τring
20	1369.5	4.6	44.1	δC—H	56	550.9	1.8	2.7	τring
21	1354.6	8.1	111.2	δC—H	57	526.4	0.1	19.7	δring
22	1331.6	9.2	7.0	δC—H	58	487.7	1.1	1.1	τring
23	1310.6	401.1	519.6	$\nu_s NO_2$	59	475.3	1.7	4.0	τring
24	1291.5	43.2	35.7	δC—H	60	462.0	18.9	0.7	τring
25	1263.0	5.4	19.7	δC—H	61	409.7	1.0	10.5	δring
26	1249.3	6.5	57.9	δC—H	62	384.7	0.5	5.1	τring
27	1220.6	0.1	37.1	δC—H	63	357.2	0.4	6.9	δring
28	1160.8	8.1	51.6	δC—H	64	342.8	0.5	8.7	δring
29	1152.0	7.7	16.0	δC—H	65	273.6	1.0	1.2	δring
30	1148.3	9.7	8.2	δC—H	66	262.1	0.1	1.8	τring
31	1132.2	9.5	2.7	δC—H	67	233.8	0.2	1.6	τring
32	1103.7	2.3	14.6	δC—H	68	163.2	0.3	1.2	τring
33	1057.1	3.6	16.1	δC—H	69	156.2	2.6	2.1	δring
34	995.7	2.5	42.0	δC—H	70	90.7	1.9	1.0	τring
35	969.7	0.0	0.8	γC—H	71	67.1	1.1	3.5	τring
36	965.4	1.9	2.2	γC—H	72	49.2	0.7	4.4	τNO_2

[a] Harmonic values corrected by a scaling factor of 0.9679 taken from Ref. [34].
[b] ν = stretching, δ = in-plane bending, γ = out-of-plane bending, σ = scissoring, τ = torsion, a = antisymmetric, s = symmetric. The relative weights of the geometrical parameters for each normal vibrational mode are given in Table S3 of the Supplementary data.

region (1000–1700 cm^{-1} wavenumber range, Fig. 7): it is calculated at 1311, 1315 and 1344 cm^{-1} for **1-NA**, **2-NA** and **9-NA**, respectively. This transition is mainly attributed to the $\nu_s NO_2$ vibration (Fig. 8a). For **2-NA** and **9-NA** the calculated $\nu_s NO_2$ wavenumbers can be compared to the experimental bands at 1342 cm^{-1} [25] and 1372–1374 cm^{-1} [26], respectively. It is worth to note that the IR intensity of this mode is dramatically influenced by the position of the substituent: the I_{IR}(**2-NA**)/I_{IR}(**1-NA**) and I_{IR}(**2-NA**)/I_{IR}(**9-NA**) ratios are 1.7 and 3.6, respectively. A similar behaviour was previously observed for nitrobenzo[*a*]pyrenes [56], nitrotriphenylenes [57] and nitronaphthalenes [58], where the I_{IR} of the $\nu_s NO_2$ mode systematically increases from the most NO_2-rotated to the planar isomers. The IR intensity of the $\nu_s NO_2$ transition has been associated to the mutagenic activity of nitroaromatic series of isomers, in relation to their different polar character [58]. It is worth to notice that as previously found for NPAH series of isomers [56–58], among the **NA**s the most mutagenic isomer (**2-NA**) exhibits the greatest $I_{IR}(\nu_s NO_2)$ value.

At highest wavenumber values, IR spectra show an absorption peak, mostly visible for the NO_2-rotated isomers. This vibration

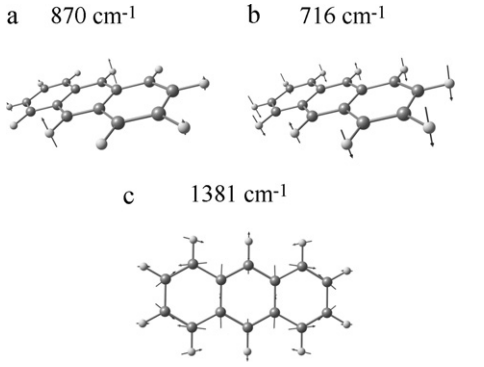

Fig. 5. Atom vector displacements for the normal modes of anthracene: (a) γC—H vibration (mode no. 42); (b) γC—H vibration (mode no. 50); (c) νring vibration (mode no. 19). B3LYP/6-311 + G** results.

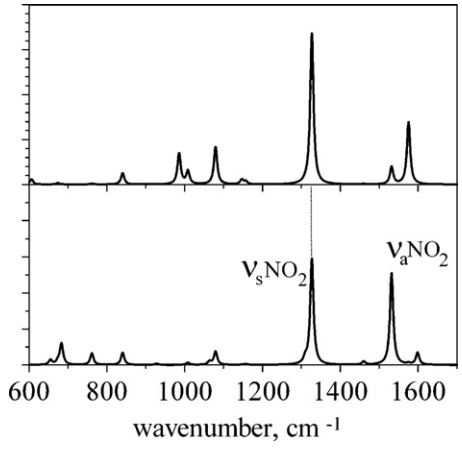

Fig. 6. Calculated B3LYP/6-311 + G** IR (bottom) and Raman (top) spectra of nitrobenzene.

Table 5
Calculated vibrational wavenumbers (cm^{-1}), IR intensities, I_{IR} (km/mol) and Raman activities, A_{Raman} ($Å^4$/amu) of 2-nitroanthracene. B3LYP/6-311+G** results.

No.	Wav. [a]	I_{IR}	A_{Raman}	Descr.[b]	No.	Wav.[a]	I_{IR}	A_{Raman}	Descr.[b]
1	3123.9	5.1	120.9	νC—H	37	949.1	3.7	2.3	γC—H
2	3107.6	1.9	55.2	νC—H	38	941.5	3.6	3.4	δring
3	3089.3	21.8	415.3	νC—H	39	912.0	32.5	1.7	γC—H
4	3078.3	23.6	133.4	νC—H	40	893.4	1.3	0.4	δring
5	3074.3	7.9	115.8	νC—H	41	879.6	16.7	0.1	γC—H
6	3067.1	0.3	187.2	νC—H	42	863.9	18.5	0.1	γC—H
7	3063.9	4.5	12.6	νC—H	43	831.7	34.1	13.0	σNO_2
8	3062.3	3.9	24.0	νC—H	44	829.8	0.2	0.0	γC—H
9	3060.2	2.6	12.2	νC—H	45	800.6	12.7	6.2	δring
10	1613.6	11.3	0.5	νring	46	795.6	5.2	0.0	γC—H
11	1606.8	59.1	428.3	νring	47	745.9	0.1	0.7	γC—H
12	1572.7	22.1	3.1	νring	48	742.4	0.0	79.1	δring
13	1553.7	30.0	48.5	νring	49	733.3	37.7	0.7	γC—H
14	1533.6	31.1	30.9	νring	50	713.1	2.1	0.2	γC—H
15	1515.6	144	22.3	$\nu_a NO_2$	51	702.2	28.1	0.6	γC—H
16	1462.6	13.3	185.3	δC—H	52	685.2	4.1	4.6	δring
17	1434.1	0.8	17.4	δC—H	53	628.5	0.5	2.7	δring
18	1421.3	2.4	6.0	δC—H	54	609.4	3.3	0.7	δring
19	1391.0	10.0	1161.2	νring	55	565.5	0.1	0.1	τring
20	1372.5	0.3	197.6	δC—H	56	547.0	4.5	3.6	δring
21	1343.1	0.8	21.4	δC—H	57	520.1	2.3	3.2	δring
22	1333.2	16.0	5.8	δC—H	58	497.7	0.2	0.2	τring
23	1315.1	684.8	1575.2	$\nu_s NO_2$	59	467.0	6.0	1.2	τring
24	1280.5	4.0	11.0	δC—H	60	455.6	19.4	0.2	τring
25	1254.5	0.1	2.6	δC—H	61	448.9	1.0	22.9	δring
26	1248.6	1.6	73.6	δC—H	62	394.6	0.2	5.8	δring
27	1240.4	9.1	35.5	δC—H	63	376.8	0.1	0.0	τring
28	1171.8	5.8	26.6	δC—H	64	294.7	0.8	7.3	δring
29	1153.3	1.2	3.4	δC—H	65	288.9	0.1	0.3	τring
30	1137.6	12.5	11	δC—H	66	258	1.5	2.1	δring
31	1126.3	0.5	6.3	δC—H	67	243.1	0.0	1.4	τring
32	1098.5	2.8	12.2	δC—H	68	157.4	2.2	0.1	τring
33	1056.1	97.8	200.7	νC—N	69	141.2	0.7	0.9	δring
34	995.8	5.4	34.6	δC—H	70	106.8	1.5	0.1	τring
35	970.0	0.0	0.5	γC—H	71	56.4	0.4	1.9	τring
36	960.3	0.6	1	γC—H	72	40.7	0.1	0.1	τNO_2

[a] Harmonic values corrected by a scaling factor of 0.9679 taken from Ref. [34].
[b] ν = stretching, δ = in-plane bending, γ = out-of-plane bending, σ = scissoring, τ = torsion, a = antisymmetric, s = symmetric. The relative weights of the geometrical parameters for each normal vibrational mode are given in Table S4 of the Supplementary data.

is mainly ascribed to the $\nu_a NO_2$ with the non-negligible contribution from a νring vibration (Fig. 8b) and is located at 1515, 1516 and 1534 cm^{-1} for **1-NA**, **2-NA** and **9-NA**, respectively. For **1-NA** and especially **2-NA** this peak is less intense than that of the $\nu_s NO_2$, while for the **9-NA** isomer the I_{IR} value for the $\nu_a NO_2$ and $\nu_s NO_2$ vibrations are comparable. It is interesting to note that, for **2-NA** the agreement between the experimental [25] and calculated wavenumber values for the $\nu_a NO_2$ mode is excellent (error of 0.1%). Note also that the low-energy spectral region

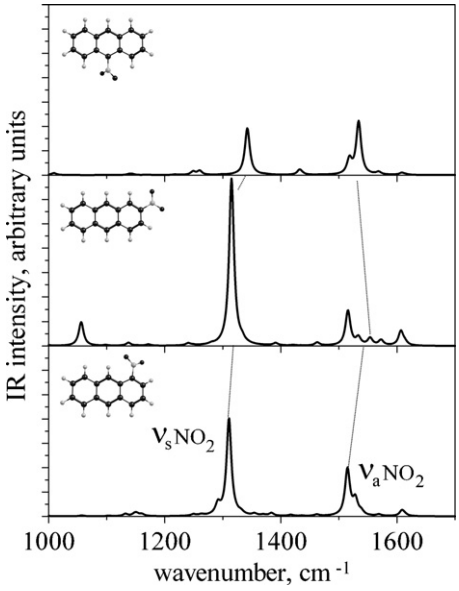

Fig. 7. Calculated B3LYP/6-311+G** IR spectra of nitroanthracene isomers.

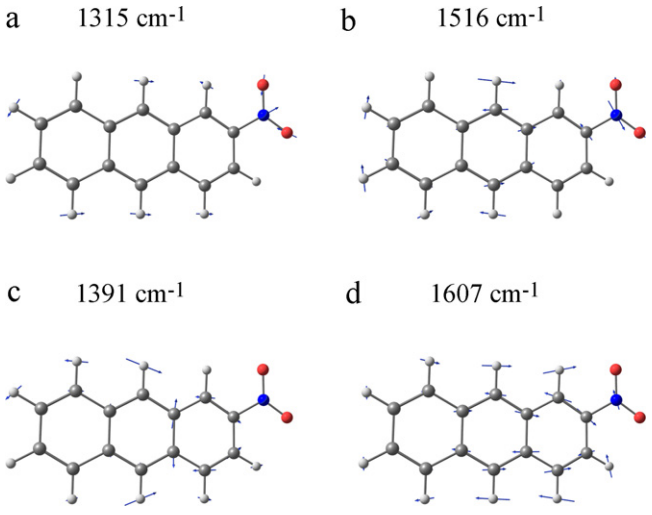

Fig. 8. Atom vector displacements of the normal modes of 2-nitroanthracene: (a) $\nu_s NO_2$ vibration (mode no. 23); (b) $\nu_a NO_2$ vibration (mode no. 15); (c) νring vibration (mode no. 19); (d) νring vibration (mode no. 11). B3LYP/6-311+G** results.

Table 6
Calculated vibrational wavenumbers (cm^{-1}), IR intensities, I_{IR} (km/mol) and Raman activities, A_{Raman} ($Å^4$/amu) of 9-nitroanthracene. B3LYP/6-311 + G** results.

No.	Wav. [a]	I_{IR}	A_{Raman}	Descr.[b]	No.	Wav.[a]	I_{IR}	A_{Raman}	Descr.[b]
1	3110.4	0.7	210.0	νC—H	37	967.6	2.2	16.1	νC—N
2	3110.1	7.5	23.4	νC—H	38	951.1	1.6	0.0	γC—H
3	3088.5	7.6	574.8	νC—H	39	948.0	0.0	3.9	γC—H
4	3088.3	27.1	42.4	νC—H	40	921.0	0.2	0.1	δring
5	3075.1	22.5	115.4	νC—H	41	884.8	26.6	0.3	γC—H
6	3074.9	0.9	145.1	νC—H	42	853.3	20.1	7.3	δring
7	3065.7	2.3	120.9	νC—H	43	850.9	0.4	0.3	δring
8	3064.5	0	19.6	νC—H	44	837.3	1.4	2.2	γC—H
9	3060.6	2.1	15.2	νC—H	45	833.1	7.2	0.4	γC—H
10	1614.9	2.4	0.2	νring	46	772.7	19.6	0.8	γC—H
11	1608.3	8.4	6.2	νring	47	765.1	22.5	48.1	σNO_2
12	1568.4	10.7	21.9	νring	48	745.0	0.5	1.5	γC—H
13	1537.1	1.0	174.8	νring	49	724.9	51.4	0.2	γC—H
14	1534.0	217.1	5.7	$\nu_a NO_2$	50	722.9	0.7	0.9	γC—H
15	1518.1	60.8	2.7	νring	51	714.5	18.9	0.2	γC—H
16	1468.8	0.9	111.5	δC—H	52	655.6	0.3	2.9	δring
17	1436.1	3.6	3.0	δC—H	53	634.4	12.5	0.6	δring
18	1432.3	20.0	0.3	δC—H	54	632.8	1.8	0.8	δring
19	1378.2	0.6	816.6	νring	55	589.0	9.9	0.4	δring
20	1372.4	1.6	0.4	δC—H	56	550.8	1.8	1.2	τring
21	1355.3	1.1	11.6	δC—H	57	512.9	9.9	7.1	δring
22	1342.3	192.4	98.8	$\nu_s NO_2$	58	482.4	0.6	1.7	τring
23	1321.1	0.4	0.7	δC—H	59	462.9	0.6	2.9	τring
24	1298.7	1.1	9.2	δC—H	60	435.5	8.1	2.0	τring
25	1260.1	16.6	2.0	δC—H	61	398.2	0.2	7.9	δring
26	1248.9	13.9	134.1	δC—H	62	393.3	0.4	34.6	δring
27	1217.7	2.3	13.3	δC—H	63	350.4	0.0	1.0	δring
28	1172.2	1.0	12.9	δC—H	64	349.3	0.0	0.3	τring
29	1166.3	0.6	9.7	δC—H	65	250.5	0.0	0.4	τring
30	1143.7	4.4	1.2	δC—H	66	225.3	0.0	2.2	τring
31	1138.3	3.3	6.0	δC—H	67	219.4	3.6	1.3	δτring
32	1094.6	0.4	0.1	δC—H	68	177.4	3.6	3.6	τring
33	1009.5	7.1	0.6	δC—H	69	111.0	0.2	0.6	τring
34	1006.3	1.6	72.5	δC—H	70	104.2	0.1	2.7	τring
35	970.4	0.1	1.5	γC—H	71	73.4	1.4	3.1	τring
36	970.1	0.0	0.2	γC—H	72	60.5	1.1	5.2	τNO_2

[a] Harmonic values corrected by a scaling factor of 0.9679 taken from Ref. [34].
[b] ν = stretching, δ = in-plane bending, γ = out-of-plane bending, σ = scissoring, τ = torsion, a = antisymmetric, s = symmetric. The relative weights of the geometrical parameters for each normal vibrational mode are given in Table S5 of the Supplementary data.

(wavenumbers < 1000 cm^{-1}) does not show relevant absorptions useful to discriminate unambiguously the **NA** isomers.

3.3. Raman spectra of nitroanthracenes

The B3LYP/6-311 + G** A_{Raman} values of the **NA** isomers are collected in Tables 4–6. As previously found for the IR spectra, both the high-wavenumber (>3000 cm^{-1}) and low-wavenumber (<1000 cm^{-1}) spectral regions are poorly dependent by the position of the NO_2 group, revealing similarities in most of the band patterns of the isomers. Thus these regions are of little utility to identify the investigated isomers. On the other hand, the medium-energy spectral region between 1000 and 1700 cm^{-1} (Fig. 9) is somewhat affected by the position of the substituent. In facts, the Raman spectrum of the **1-NA**, **2-NA** and **9-NA** isomers is characterized by the presence of two, three and one relatively intense peaks, respectively. Interestingly, for **2-NA** the intensity of the three peaks increases regularly as the wavenumber value decreases, in nice agreement with the observed Raman spectrum [25]. The $\nu_a NO_2$ mode located at 1515–1540 cm^{-1} in the IR spectra, shows only weakly or moderately intense bands in the Raman spectra (A_{Raman} = 6–68 $Å^4$/amu), in line with experiment [25]. By contrast, the $\nu_s NO_2$ vibration produces a very strong transition for **1-NA** and **2-NA**, being the most prominent peak for the latter isomer (mode no. 23, wavenumber = 1315 cm^{-1}, A_{Raman} = 1575 $Å^4$/amu). Note that, as for the I_{IR} data, the $A_{Raman}(\nu_s NO_2)$ value increases in the order **9-NA** < **1-NA** < **2-NA**, the datum for **2-NA** being one order of magnitude higher than that for the **9-NA** isomer. A quite similar situation was previously encountered in NPAH series of isomers [56–58], where the Raman intensity of the $\nu_s NO_2$ transition increases as the O—N—C—C dihedral angles decrease and the mutagenic potency increases. In a recent study [58], Raman spectra have been employed to elucidate the different mutagenic activity

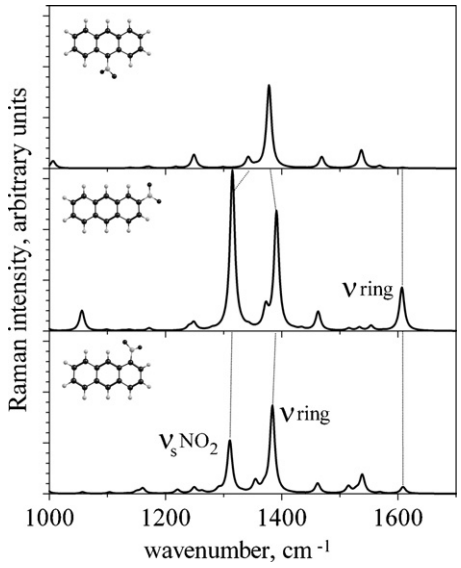

Fig. 9. Calculated B3LYP/6-311 + G** Raman spectra of nitroanthracene isomers.

of nitronaphtalene isomers. Thus, on the basis of geometrical as well as IR and Raman properties the unknown mutagenic activity of **1-NA** is predicted to be between that of **9-NA** and **2-NA** isomers.

As can be appreciated from the data reported in Tables 4–6 and shown in Fig. 9, for **1-NA** and **9-NA** the strongest Raman peak occurs at 1384 and 1378 cm^{-1}, respectively, and is attributed to a νring vibration with the contribution from C—H in-plane bending deformations. The corresponding wavenumber value for **2-NA** is computed at 1391 cm^{-1} (see the atomic displacements in Fig. 8c), with an intensity value comparable to that of the $\nu_s NO_2$ transition (Table 5, Fig. 9). This transition is very weak in the IR spectra of all the isomers. Present results show that, the wavenumber difference between the strong $\nu_s NO_2$ and νring Raman peaks is sensitive to the position of the nitro group (Tables 4–6, Fig. 9), being similar for **1-NA** and **2-NA** (*ca.* 70 cm^{-1}) but significantly smaller for the **9-NA** isomer (36 cm^{-1}). Note finally that, the Raman spectrum of **2-NA** exhibits an almost isolated and relatively intense band calculated at 1607 cm^{-1} (mode no. 11, A_{Raman} = 428 $Å^4$/amu). It is mainly attributed to νring with the contribution from the $\nu_a NO_2$ motion (Fig. 8d). The wavenumber value of this mode is predicted to be not sensitive to the substitution effect, being 1609 and 1608 cm^{-1} for the **1-NA** and **9-NA** isomers, respectively. However this transition is rather weak for **1-NA** (A_{Raman} = 65 $Å^4$/amu) and especially for **9-NA** (A_{Raman} = 6 $Å^4$/amu), making it a vibrational marker potentially useful to identify the planar **2-NA** isomer.

4. Conclusions

The IR and Raman spectra for the **1-NA**, **2-NA** and **9-NA** isomers in the ground-state were determined and analyzed at DFT level of theory using the B3LYP functional and the 6-31G* and 6-311 + G** basis sets. The relative stability increases in the order **9-NA** < **1-NA** < **2-NA** as a result of steric and consequent π-conjugative effects. High-energy (wavenumbers > 3000 cm^{-1}) and low-energy (wavenumbers < 1000 cm^{-1}) spectral regions are scarcely informative to discriminate unambiguously the investigated isomers. Both the IR and Raman intensity values of the symmetric nitro group stretching mode are sensitive to the position of the substituent, increasing significantly on going from the most NO_2-rotated **9-NA** to the planar **2-NA** structure. In the Raman spectra the number and the relative position of the most intense peaks are potentially useful to distinguish **NA** isomers. On the basis of both structural and spectroscopic properties the unknown mutagenic potency of **1-NA** is expected to be between that of **9-NA** and **2-NA** isomers.

Acknowledgements

The authors gratefully acknowledge MIUR (Rome) for financial support in the framework of PRIN2009.

Appendix A. Supplementary data

Supplementary data associated with this article can be found, in the online version, at doi:10.1016/j.saa.2011.12.052.

References

[1] J.N. Pitts, K.A. Van Cauwenberghe, D. Grosjean, J.P. Schmid, D.R. Fits, W.L. Belser, G.B. Knudson, P.M. Hynds, Science 202 (1978) 515–519.
[2] H. Tokiwa, Y. Ohnishi, Crit. Rev. Toxicol. 17 (1986) 23–60.
[3] P.P. Fu, Drug Metab. Rev. 22 (1990) 209–268.
[4] H. Yu, J. Environ. Sci. Health C 20 (2002) 149–183.
[5] T.L. Gibson, Atmos. Environ. 16 (1982) 2037–2040.
[6] B.J. Finlayson-Pitts, J.N. Pitts, Science 276 (1997) 1045–1051.
[7] R. Atkinson, J. Arey, Environ. Health Perspect. 102 (1994) 117–126.
[8] J. Arey, Atmospheric reactions of PAHs including formation of nitroarenes, in: A.H. Neison (Ed.), PAHs and Related Compounds, Springer-Verlag, Berlin, Germany, 1998, p. 347.
[9] J. Trotter, Acta Crystallogr. 12 (1959) 237–242.
[10] O.L. Chapman, D.C. Heckert, J.W. Reasoner, S.P. Thackaberry, J. Am. Chem. Soc. 88 (1966) 5550–5554.
[11] K. Hamanoue, T. Nakayama, K. Kajiwara, S. Yamanaka, K. Ushida, J. Chem. Soc. Faraday Trans. 88 (1992) 3145–3151.
[12] R. Morales-Cueto, M. Esquivelzeta-Rabell, J. Saucedo-Zugazagoitia, J. Peon, J. Phys. Chem. A 111 (2007) 552–557.
[13] S.D. Warner, J.P. Farant, I.S. Butler, Chemosphere 54 (2004) 1207–1215.
[14] S.-T. Lin, Y.-F. Jih, P.P. Fu, J. Org. Chem. 61 (1996) 5271–5273.
[15] K.K. Onchoke, C.M. Hadad, P.K. Dutta, Polycycl. Aromat. Comp. 24 (2004) 37–64.
[16] S.-L. Lee, K.-C. Yang, J.-H. Sheu, Y.-J. Lu, Int. J. Quantum Chem. Quantum Chem. Symp. 29 (1995) 509–522.
[17] P.P. Fu, Y. Zhang, Y.-L. Mao, L.S. Von Tungeln, Y. Kim, H. Jung, M.J. Jun, J. Chromatogr. A 642 (1993) 107–116.
[18] H. Tokiwa, R. Nakagawa, Y. Ohnishi, Mutation Res. 91 (1981) 321–325.
[19] J.N. Pitts Jr., D.M. Lokensgard, W. Harger, T.S. Fisher, V. Mejia, J.J. Schuler, G.M. Scorziell, Y.A. Katzenstein, Mutation Res. 103 (1982) 241–249.
[20] H.S. Rosenkranz, R. Mermelstein, Mutation Res. 114 (1983) 217–267.
[21] P.P.Fu, L.S. Von Tungeln, M.W. Chou, Carcinogenesis 6 (1985) 753–757.
[22] H. Jung, A.U. Shaikh, R.H. Heflich, P.P. Fu, Environ. Mol. Mutag. 17 (1991) 169–180.
[23] B.A. Hess Jr., J. Schaad, P. Carsky, R. Zahradnik, Chem. Rev. 86 (1986) 709–730.
[24] P. Pulay, X. Zhou, G. Fogarasi, in: R. Fausto (Ed.), Recent Experimental and Computational Advances in Molecular Spectroscopy, Kluwer Academic, Netherlands, 1993, pp. 99–112.
[25] Y.S. Li, P.P. Fu, J.S. Church, J. Mol. Struct. 550–551 (2000) 217–223.
[26] J. Trotter, Can. J. Chem. 37 (1959) 1009–1011, and references therein.
[27] M.J. Frisch, G.W. Trucks, H.B. Schlegel, G.E. Scuseria, M.A. Robb, V.G. Cheeseman, J.A. Montgomery, T. Vreven Jr., K.N. Kudin, J.C. Burant, J.M. Millam, S.S. Iyengar, J. Tomasi, V. Barone, B. Mennucci, M. Cossi, G. Scalmani, N. Rega, G.A. Petersson, H. Nakatsuji, M. Hada, M. Ehara, K. Toyota, R. Fukuda, J. Hasegawa, M. Ishida, T. Nakajima, Y. Honda, O. Kitao, H. Nakai, M. Klene, X. Li, J.E. Knox, H.P. Hratchian, J.B. Cross, C. Adamo, J. Jaramillo, R. Gomperts, R.E. Stratmann, O. Yazyev, A.J. Austin, R. Cammi, C. Pomelli, J.W. Ochterski, P.Y. Ayala, K. Morokuma, G.A. Voth, P. Salvador, J.J. Dannenberg, V.G. Zakrzewski, S. Dapprich, A.D. Daniels, M.C. Strain, O. Farkas, D.K. Malick, A.D. Rabuck, K. Raghavachari, J.B. Foresman, J.V. Ortiz, Q. Cui, A.G. Baboul, S. Clifford, J. Cioslowski, B.B. Stefanov, G. Liu, A. Liashenko, P. Piskorz, I. Komaromi, R.L. Martin, D.J. Fox, T. Keith, M.A. Al-Laham, C.Y. Peng, A. Nanayakkara, M. Challacombe, P.M.W. Gill, B. Johnson, W. Chen, M.W.Wong, C. Gonzalez, J.A. Pople, GAUSSIAN 03, revision B.03, Gaussian, Inc., Pittsburgh, PA, 2003.
[28] C. Lee, A.D. Yang, R.G. Parr, Phys. Rev. B 37 (1988) 785–789.
[29] A.D. Becke, J. Chem. Phys. 98 (1993) 1372–1377.
[30] J.M. Bowman, J. Chem. Phys. 68 (1978) 608–610.
[31] V. Barone, J. Chem. Phys. 122 (2005) 014108–014117.
[32] P. Pulay, G. Fogarasi, G. Pongor, J.E. Boggs, A. Vargha, J. Am. Chem. Soc. 105 (1983) 7037–7047.
[33] K.K. Irikura, R.D. Johnson, R.N. Kacker, J. Phys. Chem. A 109 (2005) 8430–8437.
[34] M.P. Andersson, P. Uvdal, J. Phys. Chem. A 109 (2005) 2937–2941.
[35] V. Librando, A. Alparone, Polycycl. Aromat. Comp. 27 (2007) 65–94.
[36] K.C. Gordon, G. David, T.J. Walsh, Spectrochim. Acta A 72 (2009) 209–213.
[37] S. Chandra, H. Saleem, N. Sundaraganesan, S. Sebastian, Spectrochim. Acta A 74 (2009) 704–713.
[38] V. Librando, A. Alparone, J. Hazard. Mater. 161 (2009) 1338–1346.
[39] P.B. Nagabalasubramanian, S. Periandy, Spectrochim. Acta A 77 (2010) 1099–1107.
[40] D.A. Dhas, I.H. Joe, S.D.D. Roy, S. Balachandran, Spectrochim. Acta A 79 (2011) 993–1003.
[41] A. Chandran, Y.S. Mary, H.T. Varghese, C.Y. Panicker, P. Pazdera, G. Rajendran, Spectrochim. Acta A 79 (2011) 1584–1592.
[42] Z. Li, W. Deng, Spectrochim. Acta A 82 (2011) 56–62.
[43] G.A. Zhurko, D.A. Zhurko, Chemcraft, http://www.chemcraftprog.com.
[44] A. Domenicano, G. Schultz, I. Hargittai, M. Colapietro, G. Portalone, P. George, C.W. Bock, Struct. Chem. 1 (1990) 107–122.
[45] P.D. Enlow, T. Vo-Dinh, Anal. Chem. 58 (1986) 1119–1123.
[46] J.M.L. Martin, J. El-Yazal, J.-P. Francois, J. Phys. Chem. 100 (1996) 15358–15367.
[47] E. Cané, A. Miani, P. Calmieri, R. Tarroni, A. Trombetti, J. Chem. Phys. 06 (1997) 9004–9012, and references therein.
[48] C.W. Bauschlicher, S.R. Langhoff, Spectrochim. Acta A 53 (1997) 1225–1240.
[49] J. Clarkson, W.E. Smith, J. Mol. Struct. 655 (2003) 413–422.
[50] V. Krishnakumar, S. Muthunatesan, Spectrochim. Acta A 61 (2005) 199–204.
[51] V. Krishnakumar, R.J. Xavier, Spectrochim. Acta A 61 (2005) 1799–1809.
[52] V. Krishnakumar, N. Prabavathi, S. Muthunatesan, Spectrochim. Acta A 70 (2008) 991–996.
[53] M. Arivazhagan, V. Krishnakumar, R.J. Xavier, G. Ilango, V. Balachandran, Spectrochim. Acta A 72 (2009) 941–946.
[54] C.D. Keefe, J.E. Pickup, Spectrochim. Acta A 72 (2009) 947–953.
[55] C. Ravikumar, L. Padmaja, I.H. Joe, Spectrochim. Acta A 75 (2010) 859–866.
[56] K.K. Onchoke, C.M. Hadad, P.K. Dutta, J. Phys. Chem. A 110 (2006) 76–84.
[57] K.K. Onchoke, M.E. Parks, A.H. Nolan, Spectrochim. Acta A 74 (2009) 579–587.
[58] V. Librando, A. Alparone, J. Hazard. Mater. 154 (2008) 1158–1165.